Biochemistry

Article

Cite This: Biochemistry 2018, 57, 620–630

pubs.acs.org/biochemistry

Variation in LOV Photoreceptor Activation Dynamics Probed by Time-Resolved Infrared Spectroscopy

James N. Iuliano,[†] Agnieszka A. Gil,[†] Sergey P. Laptenok,[‡,@] Christopher R. Hall,[‡] Jinnette Tolentino Collado,[†] Andras Lukacs,[‡,§] Safaa A. Hag Ahmed,[†] Jenna Abyad,[†] Taraneh Daryaee,[†] Gregory M. Greetham,[∥] Igor V. Sazanovich,[∥] Boris Illarionov,[#] Adelbert Bacher,[⊥] Markus Fischer,[#] Michael Towrie,[∥] Jarrod B. French,[†] Stephen R. Meech,*[,‡] and Peter J. Tonge*[,†]

[†]Department of Chemistry, Stony Brook University, Stony Brook, New York 11794, United States

[‡]School of Chemistry, University of East Anglia, Norwich NR4 7TJ, U.K.

[§]Department of Biophysics, Medical School, University of Pecs, Szigeti út 12, 7624 Pecs, Hungary

[∥]Central Laser Facility, Research Complex at Harwell, Rutherford Appleton Laboratory, Didcot OX11 0QX, U.K.

[⊥]Department Chemie, Technische Universität München, D-85747 Garching, Germany

[#]Institut für Biochemie und Lebensmittelchemie, Universität Hamburg, Grindelallee 117, D-20146 Hamburg, Germany

Supporting Information

ABSTRACT: The light, oxygen, voltage (LOV) domain proteins are blue light photoreceptors that utilize a noncovalently bound flavin mononucleotide (FMN) cofactor as the chromophore. The modular nature of these proteins has led to their wide adoption in the emerging fields of optogenetics and optobiology, where the LOV domain has been fused to a variety of output domains leading to novel light-controlled applications. In this work, we extend our studies of the subpicosecond to several hundred microsecond transient infrared spectroscopy of the isolated LOV domain AsLOV2 to three full-length photoreceptors in which the LOV domain is fused to an output domain: the LOV-STAS protein, YtvA, the LOV-HTH transcription factor, EL222, and the LOV-histidine kinase, LovK. Despite differences in tertiary structure, the overall pathway leading to cysteine adduct formation from the FMN triplet state is highly conserved, although there are slight variations in rate. However, significant differences are observed in the vibrational spectra and kinetics after adduct formation, which are directly linked to the specific output function of the LOV domain. While the rate of adduct formation varies by only 3.6-fold among the proteins, the subsequent large-scale structural changes in the full-length LOV photoreceptors occur over the micro- to submillisecond time scales and vary by orders of magnitude depending on the different output function of each LOV domain.

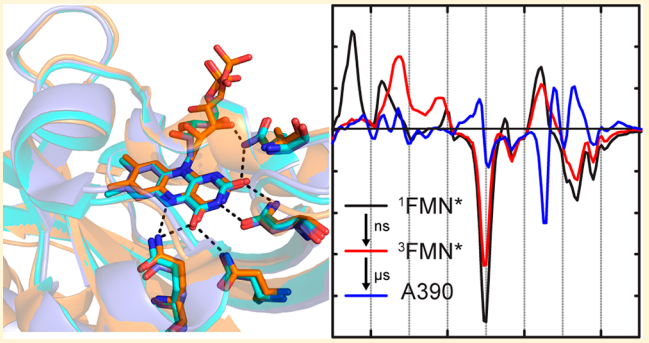

The light, oxygen, voltage (LOV) domain is part of the PAS domain superfamily and functions in a variety of light-activated biological activities, including phototropism, gene regulation, and stress response.[1] The LOV domain binds the oxidized flavin mononucleotide (FMN) in a highly conserved hydrogen bonding network composed of two Asn and two Gln residues.[2] Changes in the LOV domain upon blue light illumination occur because of the formation of a covalent adduct between C4a of FMN and a conserved Cys concomitant with protonation of N5 of FMN (Figure S1).[3] Adduct formation leads to rotation of a conserved Gln residue (Gln513 in AsLOV2), which is thought to initiate large-scale structural changes by perturbing interactions with the LOV β-sheet (Figure 1A).[3,4] Together, these events lead to activation of an effector domain, initiating biological activity.[5] Despite more than a decade of intense research on LOV photoactivation, the mechanistic link between the ultrafast structural changes around the chromophore and the structural dynamics at longer time scales remains to be fully elucidated.[6]

The modularity of the LOV domain enables blue light control of a variety of biological functions. For example, in *Avena sativa*, light activation of the LOV domain (AsLOV2) is coupled to unfolding of the Jα helix, which results in activation of a Ser/Thr kinase in the full-length phototropin.[8] AsLOV2 has also been used as a tool in the emerging field of optobiology. The AsLOV2 domain has been fused to the GTPase Rac1, where it functions as a photocage for the enzyme,[9] and also as the phototrigger for the light-inducible

Received: October 13, 2017
Revised: December 12, 2017
Published: December 14, 2017

DOI: 10.1021/acs.biochem.7b01040
Biochemistry 2018, 57, 620–630

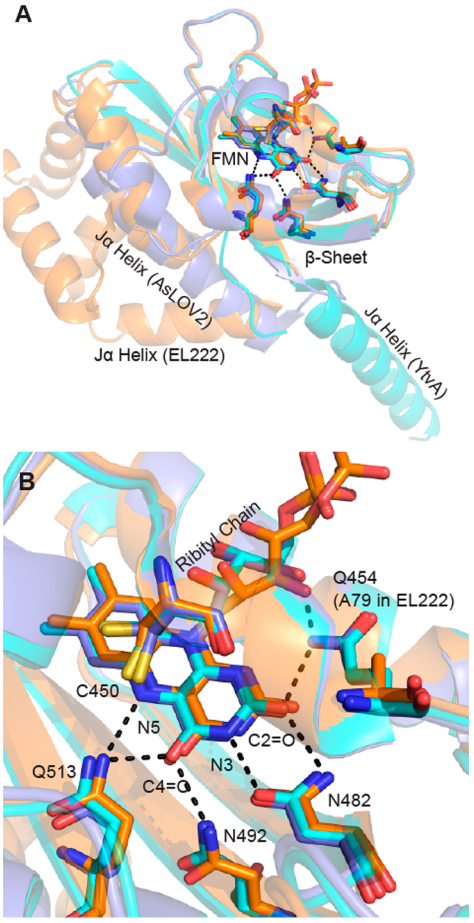

Figure 1. Superposition of LOV photoreceptor structures. The X-ray structures of AsLOV2 (2V0U, slate blue), YtvA (2PR5, cyan), and EL222 (3P7N, orange) have been superimposed using PyMOL.[7] No structure is currently available for LovK. (A) The Jα helix adopts different positions relative to the FMN binding pocket in each photoreceptor. In AsLOV2, the Jα helix is docked to the β-sheet, while this surface is occupied by the helix−turn−helix (HTH) domain in EL222 in the dark state and acts as a dimerization site in the EL222 light state. In YtvA, the β-sheet acts as the obligate dimerization site in both light and dark states, with the Jα helix extending out to the STAS domain (which is not present in this structure). (B) The flavin binding pocket is comprised of several conserved residues that interact with the flavin through hydrogen bonds. These include Q513, N492, N482, and Q454 in AsLOV2; Q123, N104, N94, and Q66 in YtvA; and Q138, N117, N107, and A79 in EL222. Residues are numbered on the basis of the sequence of AsLOV2.

dimerization system iLID.[10] The picosecond to nanosecond time-resolved infrared (TRIR) spectra of AsLOV2 in H_2O buffer were reported by both Alexandre et al. and Pfeifer et al.; the spectrum of 3FMN* was resolved using transient infrared (IR) and step-scan IR, respectively.[11,12] Recently, we and others have measured the picosecond to millisecond TRIR spectra of AsLOV2, and we have fully assigned the spectra using isotope editing by labeling the protein and the FMN cofactor.[13,14] In addition, a global fit of the data enabled the resolution of dispersive kinetics in triplet state decay to adduct formation.[13]

In this work, we now extend our analysis to three photoreceptors in which the LOV domain is fused to an output partner via the Jα helix: YtvA from *Bacillus subtilis*, which includes a sulfate transporter anti-sigma factor agonist (STAS) domain, LovK from *Caulobacter crescentus*, which includes a histidine kinase (HK) domain, and EL222 from *Erythrobacter litoralis*, which includes a helix−turn−helix (HTH) DNA binding domain. In YtvA and LovK, photoactivation is thought to involve a tilt and rotation around a dimerization site without large-scale secondary structure changes.[5,15,16] In contrast, in EL222, photoactivation results in undocking of the HTH domain from the LOV β-sheet and formation of a head-to-head DNA binding homodimer.[17,18] These four proteins show very different steady state recovery lifetimes at 25 °C: 27 s for AsLOV2,[19] 75 min for YtvA,[20] 2 h for LovK,[16] and 25 s for EL222.[21]

The flavin binding pocket is composed of several conserved residues that have noncovalent interactions with the isoalloxazine ring of FMN. Q513 and N492 are hydrogen bonded to the FMN C4═O and N5 groups, while Q454 and N482 form a network around the FMN N3 and C2═O groups (Figure 1B). Previous studies have shown that mutation of the Gln to Ala suppresses large-scale structural changes in the protein,[3,22] while mutation of the Asn residues primarily results in a lower adduct yield and modulation of triplet decay kinetics.[23] Additionally, Q454 also forms a hydrogen bond with the C2═O group and the ribityl chain of FMN in AsLOV2 and YtvA; however, this residue is an Ala in EL222.[17] An α-helix, located above the FMN chromophore, contains the conserved Cys residue that is required for LOV photocycling and forms an adduct with the photoexcited FMN that is characterized by an absorption band at 390 nm in the light state [A390 (Figure S1)].

Several studies have focused on elucidating the structural changes in LOV photoreceptors on the microsecond to millisecond time scale. Initial characterization of *Arabidopsis thaliana* Phot1 LOV2 by the thermal grating method revealed a 2 ms time constant for the unfolding of the Jα helix,[24] which was further extended to include a two-step mechanism.[25] In YtvA, it was proposed that the structural changes that could be resolved by circular dichroism are minimal and that smaller-scale changes in hydrogen bonding or salt bridge interactions are occurring as part of the activation mechanism.[26,27] More recently, the thermal grating technique has been applied to YtvA constructs lacking the effector domain, and it was found that structural changes are confined to the Jα helices.[28]

In this study, the femtosecond to millisecond dynamics of LOV photoreceptor activation have been probed using time-resolved IR with the femtosecond to millisecond time-resolved multiple-probe spectroscopy (TRMPS) method and Fourier transform infrared spectroscopy (FTIR). This has enabled the interrogation of the structural dynamics that link the initial photochemistry to generation of the signaling state in the three full-length photoreceptors.

MATERIALS AND METHODS

Protein Constructs. The truncated gene containing residues 404−546 of *A. sativa* phototropin (herein termed AsLOV2) and the genes for full-length YtvA and LovK were cloned into pET15b (Novagen) in frame with an N-terminal six-His tag. The gene containing full-length EL222 was codon-optimized, synthesized, and subcloned into pET15b by Genscript, Inc. (Piscataway, NJ).

Expression and Purification of AsLOV2, YtvA, and LovK. BL21 (DE3) (Novagen) competent *Escherichia coli* cells were transformed with the respective plasmids by heat shock and plated on LB-Agar (Diffco) supplemented with 200 μg/mL ampicillin (Gold Biosciences). After incubation overnight at 37

DOI: 10.1021/acs.biochem.7b01040
Biochemistry 2018, 57, 620−630

°C, a single colony was used to inoculate 10 mL of 2X-YT medium containing 200 μg/mL ampicillin, which was then incubated in an orbital shaker (250 rpm) at 37 °C for 2−3 h. This starter culture was then used to inoculate 1 L of 2X-YT (IBI Sci) containing 200 μg/mL ampicillin, which was then incubated under the same conditions as the starter culture until the OD_{600} reached 1.0. Protein expression was then induced by the addition of 1 mM isopropyl β-D-1-thiogalactopyranoside (Gold Biosciences), and the culture was shaken at 20 °C for 16 h. Subsequently, the cells were harvested by centrifugation at 12000*g* and then frozen at −20 °C until they were needed.

The frozen cell pellets were resuspended in 40 mL of 20 mM Tris buffer (pH 8.0) containing 150 mM NaCl (resuspension buffer), and the cells were then disrupted using a French press (Constant Systems Cell Disruptor) at a pressure of 27K psi using a cell that was maintained at 4 °C. After the addition of 100 μM phenylmethandsulfonyl fluoride (PMSF) and 20 μL of β-mercaptoethanol, the lysate was clarified by ultracentrifugation at 250000*g* for 30 min. A 3 mL Ni-NTA (Novagen) column was prepared by equilibrating the resin with resuspension buffer, and the clarified lysate was loaded onto the column. The column was washed with 100 mL of resuspension buffer and eluted using a step gradient of resuspension buffer containing 10, 20, 30, and 500 mM imidazole. Fractions containing the purified protein were pooled and dialyzed against 20 mM Tris buffer (pH 8.0) containing 150 mM NaCl. In each case, the proteins were shown to be ≥95% pure by sodium dodecyl sulfate−polyacrylamide gel electrophoresis (SDS−PAGE). Purified and desalted protein fractions were lyophilized and dissolved in D_2O (Cambridge Isotope Laboratories) prior to measurement.

Expression and Purification of EL222. EL222 was expressed and purified using the method described above with the following modifications. After the clarified cell extract had been loaded onto the Ni-NTA column, the bound protein was first washed with resuspension buffer and then eluted using resuspension buffer containing 5 mM imidazole. Fractions containing the protein were pooled and dialyzed overnight into 20 mM Tris buffer (pH 7.6) containing 30 mM NaCl. The dialyzed protein was then loaded onto a 5 mL Q-Sepharose column that had been equilibrated with the same buffer. The eluent was reloaded onto the column to maximize the amount of EL222 that bound to the resin. The protein was eluted using a gradient from 30 to 500 mM NaCl in 20 mM Tris buffer (pH 7.6). Fractions containing EL222 were pooled, and the protein was shown to be ≥95% pure by SDS−PAGE. Purified and desalted EL222 was lyophilized and suspended in D_2O prior to measurement.

Time-Resolved Multiple-Probe Spectroscopy (TRMPS). TRMPS measurements were conducted at the Central Laser Facility of the Rutherford Appleton Laboratory using the apparatus described previously.[29] Briefly, 800 nJ pulses of the 450 nm pump excitation wavelength were provided by a Ti:sapphire laser-pumped OPA at a rate of 1 kHz with a pulse duration of 100 fs. A broadband mid-IR probe was generated using a 10 kHz Ti:sapphire laser pumping an OPA with a difference frequency generation (DFG) stage. The signal and idler outputs of the OPA were mixed to form the mid-IR broadband probe pulse with a duration of <100 fs. Two MCT detectors were used for data collection and gave an ∼400 cm^{-1} spectral bandwidth with 3 cm^{-1} resolution. The spectra were calibrated using transmission of a polystyrene film. To avoid photodegradation and conversion to the light state, the sample was passed through a Harrick cell with CaF_2 windows and a 50 μm spacer. The flow rate was set to 1 mL/min, and the cell was rastered in the beam to minimize unwanted secondary photochemistry. Data were analyzed by global analysis using the Glotaran Software Package that globally fits a selected kinetic model to the entire time-resolved spectral data set; in the case presented hee, we fit a sequential first-order model to the data.[30]

Fourier Transform Infrared Spectroscopy (FTIR). FTIR spectra were recorded on a Bruker Vertex80 instrument modified to accommodate a light-emitting diode (LED) and a temperature-controlled sample holder to maintain the sample temperature at 20 °C. Dark state spectra were recorded at 1 cm^{-1} resolution, and 128 scans were collected and averaged. The light state was generated after irradiation for 2 min at 450 nm using the LED, and the dark state spectrum was subtracted from the light state spectrum to generate the difference spectrum.

RESULTS

In this study, we have characterized the activation of the LOV domain from the initial dark state structure to the final light state structure. Below we compare time-resolved infrared difference spectra (TRIR) tracking the conversion from the singlet excited state (^{1}FMN*, nanosecond time scale) to the triplet state (^{3}FMN*, microsecond time scale), then adduct formation (A390), and finally the subsequent protein structural evolution (microsecond to millisecond time scale).

TRIR spectra of YtvA, LovK, and EL222, together with AsLOV2, are shown in Figure 2. Negative signals (bleaches) correspond to depopulated ground state modes, and positive transients are vibrational modes arising from the excited state or new ground state populations. Evolution-associated spectra (EAS) of the four LOV proteins were subsequently determined from a sequential decay model globally fit to the experimental TRIR data (Figure 3); the quality of the fit is shown in Figure S2. The data for each of the proteins are shown as a heat map with the time on the *y*-axis and wavenumber on the *x*-axis with a color bar showing approximate intensity values. Horizontal lines denote the three major phases of the LOV photocycle that can be resolved in the TRMPS experiment: ^{1}FMN*, ^{3}FMN*, and A390. Below we compare the EAS for the three full-length LOV proteins with the EAS for AsLOV2 that we recently published.[13] We first briefly review the time-resolved vibrational spectrum of AsLOV2 as a foundation for the subsequent discussion.

The first EAS (Figure 3A, black line) shows the instantaneously formed singlet excited state of FMN (^{1}FMN*) in AsLOV2. This excited state is characterized by positive transients at ∼1375 and ∼1413 cm^{-1} and ground state bleaches at ∼1550 and ∼1580 cm^{-1} assigned to the C10a−N1 and C4a−N5 FMN modes, respectively.[13,31,32] In addition, signals in the 1600−1660 cm^{-1} region can be assigned to overlapping flavin (C2═O) and protein modes, while bleaches at 1690 and 1705 cm^{-1} are assigned to Q513 and the FMN C4═O group, respectively.[13] The second EAS forms with an ∼2 ns time constant (Figure 3A, red line) and shows the triplet excited state (^{3}FMN*) that is evident in the disappearance of excited state transients at 1375 and 1413 cm^{-1} and the concomitant rise of transients at 1438 and 1491 cm^{-1} associated with vibrations involving the isoalloxazine moiety. ^{3}FMN* decays in 9.5 μs during the formation of an adduct

DOI: 10.1021/acs.biochem.7b01040
Biochemistry 2018, 57, 620−630

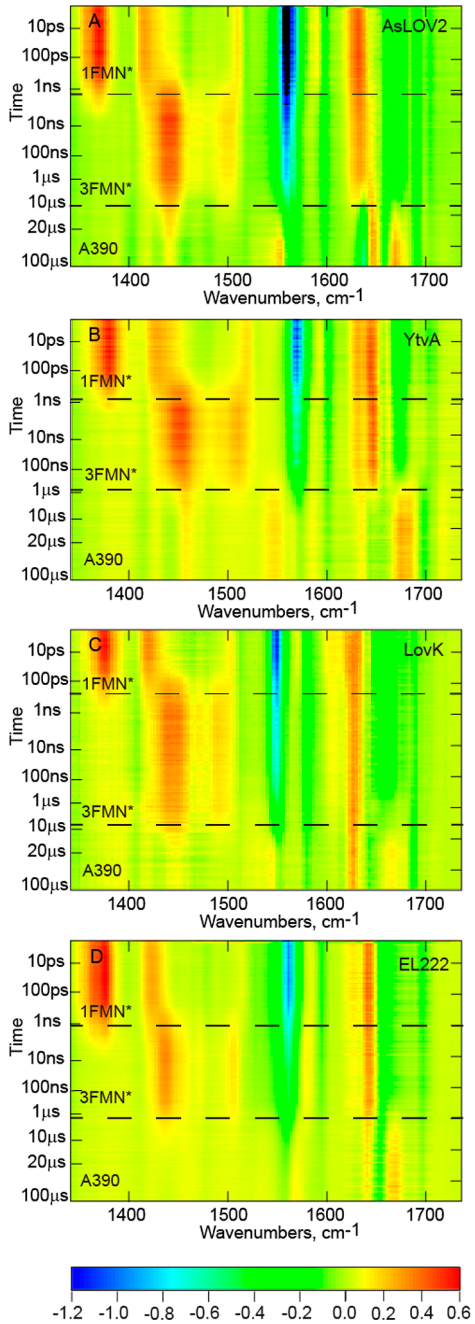

Figure 2. TRIR spectra of LOV photoreceptors (A) AsLOV2, (B) YtvA, (C) LovK, and (D) EL222 are displayed as two-dimensional heat maps with time on the *y*-axis and frequency on the *x*-axis. A color bar legend is shown below with approximate Δ*A* values for each of the normalized heat maps.

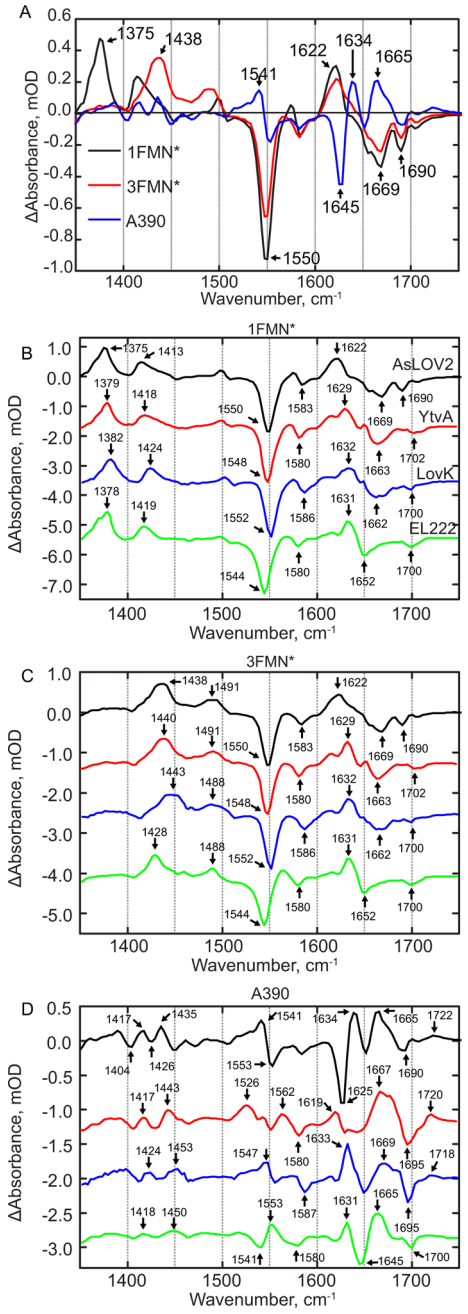

Figure 3. EAS analysis of LOV photoreceptors. (A) The EAS of AsLOV2 is shown overlaid. EAS corresponding to (B) ^{1}FMN*, (C) ^{3}FMN*, and (D) A390 are shown on a stacked *y*-axis plot. Small differences are observed in the singlet and triplet excited states, while more significant differences are reflected in the A390 spectrum and show the most variation among the four LOV proteins. Data for AsLOV2 are colored black, data for YtvA red, data for LovK blue, and data for EL222 green.

between Cys450 and FMN C4a (A390), which is characterized by a difference spectrum in which large changes in protein modes are observed (Figure 3A, blue line).[13]

EAS Comparison of Picosecond to Submillisecond Structural Dynamics. EAS were plotted on a stacked *y*-axis to facilitate direct and convenient comparison among the four wild-type proteins (Figure 3B–D). The EAS for YtvA and LovK most closely resemble the EAS for AsLOV2 (Figure 3B,C, red and blue lines, respectively). The first EAS for YtvA (Figure 3B, red line) shows the ^{1}FMN* excited state. Transients assigned to ring modes are observed at 1379 and 1418 cm^{-1}, ~4 cm^{-1} blue-shifted compared to those of AsLOV2, while the strong bleach at 1548 cm^{-1} is within the 3 cm^{-1} resolution of the experiment except for EL222, in which the strong bleach is observed at 1544 cm^{-1}.

The most significant variation between the ^{1}FMN* state of AsLOV2 and the other three proteins is found in the 1600–1670 cm^{-1} region, where the composite transient at 1622 cm^{-1} in AsLOV2 is split into at least three distinct transients in YtvA, with the most intense absorption shifted by 7 cm^{-1} to 1629 cm^{-1} with shoulders at 1615 and 1650 cm^{-1}. In LovK, a

DOI: 10.1021/acs.biochem.7b01040
Biochemistry 2018, 57, 620–630

doublet peak similar to that of YtvA is observed with frequencies of 1610 and 1632 cm^{-1} and in EL222 at 1615 and 1631 cm^{-1}. The bleach in this region of the YtvA spectrum is shifted by 6 cm^{-1} to 1663 cm^{-1} compared to that of AsLOV2, and the modes associated with Gln123 and the FMN C4═O group are merged to form a single bleach at 1702 cm^{-1}. In LovK, a bleach is observed at 1669 cm^{-1}, similar to that found in AsLOV2; however, a lower-frequency shoulder is present at 1656 cm^{-1}, while in LovK, this shoulder is observed at 1663 cm^{-1}. The EAS of ^{3}FMN* in YtvA (Figure 3C, red line) is similar to that of AsLOV2 and shows the disappearance of ^{1}FMN* transients and the appearance of ^{3}FMN* transients at 1440 and 1491 cm^{-1}, with all other protein/flavin modes changing only in intensity.

The A390 EAS shows the largest differences among the four proteins. Perhaps most interesting is the C4−C10a ring stretching vibration that is found at 1553 cm^{-1} (−)/1541 cm^{-1} (+) in AsLOV2 and YtvA. This vibrational mode was previously assigned by ^{13}C labeling of the chromophore, for which numbering in shown in the Supporting Information.[13] In YtvA, the intensity of the transient at 1553 cm^{-1} is greatly diminished because of the presence of a new transient at 1526 cm^{-1}, which is not found in the three other proteins. The 1526 cm^{-1} transient may represent either an N−C stretch or a N−D bend vibration based on FTIR spectra of [apoprotein-^{15}N]YtvA (Figure S3) and could be due to dimerization, as a similar but weaker transient is also found in LovK. In LovK, the corresponding transient is shifted by 6 cm^{-1} to 1547 cm^{-1}, while in EL222, this bleach/transient pair appears to be reversed, with the transient at 1550 cm^{-1} and the bleach at a lower frequency (1535 cm^{-1}).

Some aspects of the adduct spectra are common to the LOV proteins, such as the protein/FMN transient centered at ∼1665 cm^{-1}; however, there is some variation in the shape of the band, suggesting that a portion of this band arises from a protein mode that is not conserved. The bleach at 1625 cm^{-1} in AsLOV2 was previously assigned to the β-sheet and the adjacent transient at 1634 cm^{-1} to the α-helix.[14] This β-sheet mode appears to be blue-shifted in EL222 to 1645 cm^{-1} and in LovK to 1650 cm^{-1}. In YtvA, there is no defined bleach in this region; rather, there is a broad feature from ∼1630 to 1650 cm^{-1} that could reflect the lack of changes in the Jα helix upon signaling state formation. Application of a 70 μs component to the kinetic analysis of YtvA based on the work of Choi et al.[28] revealed the presence of a small bleach at 1642 cm^{-1} (Figure S3). While this bleach can tentatively be assigned to the Jα helix, we note that the entire spectrum changes in intensity on this time scale, complicating a full analysis of the data. Finally, a transient assigned to the C4═O group is observed after adduct formation and is found at 1722 cm^{-1} (AsLOV2), 1720 cm^{-1} (YtvA), 1718 cm^{-1} (LovK), and 1719 cm^{-1} (EL222).

Structural Differences in EL222 Are Evident from Excited State Spectra. The EAS of EL222 shows the most changes when compared to the EAS of the other LOV domain proteins (Figure 3D). In the first EAS (black line), the frequency of the ground state bleach is red-shifted to 1544 cm^{-1} compared to 1550 ± 2 cm^{-1} in the other LOV domains. Notably, this is not accompanied by any major changes in the excited state transients at 1378 and 1419 cm^{-1} that are within 3 cm^{-1} of the position observed in AsLOV2, and thus within the resolution of the experiment. The 1600−1690 cm^{-1} region is much less complex in EL222 than in the other LOV proteins. A single strong transient/bleach pair is observed at 1631(+)/1652(−) cm^{-1}, whereas multiple bands are observed in the EAS of the other proteins. In addition, the bleach at 1700 cm^{-1} is more similar to that found in YtvA and LovK in which there is only one bleach in this region assigned to the conserved Gln (Gln513 in AsLOV2).

In EL222, the transients at 1378 and 1419 cm^{-1} arising from the ^{1}FMN* state are found in essentially the same position as in AsLOV2; however, the lower-frequency ^{3}FMN* transient is shifted by 10 cm^{-1} to 1429 cm^{-1}, while the higher-frequency transient at 1488 cm^{-1} is within 3 cm^{-1} of the position observed in the other proteins. Upon adduct formation, the C4−C10a vibrational mode is perturbed and a bleach/transient pair is formed at 1541(−)/1553(+) cm^{-1}. However, unlike the other proteins, this bleach/transient is reversed in EL222 with the transient at a frequency lower than that of the bleach [i.e., 1541(+)/1553(−) cm^{-1}]. Transients in the 1600−1690 cm^{-1} region are also observed at 1631 and 1665 cm^{-1} and are assigned to protein modes, while bleaches at 1645 and 1700 cm^{-1} are assigned to modes arising from the β-sheet and Gln138, respectively.

A79Q-EL222. To resolve a possible cause of the differences between EL222 and the other LOV proteins, we prepared the A79Q-EL222 mutant to restore the Gln known to interact with the C2═O group and the FMN ribityl chain in AsLOV2, LovK, and EL222 (Figure 1). The EAS of A79Q-EL222 and wild-type EL222 are compared in Figure 4. In the ^{1}FMN* EAS

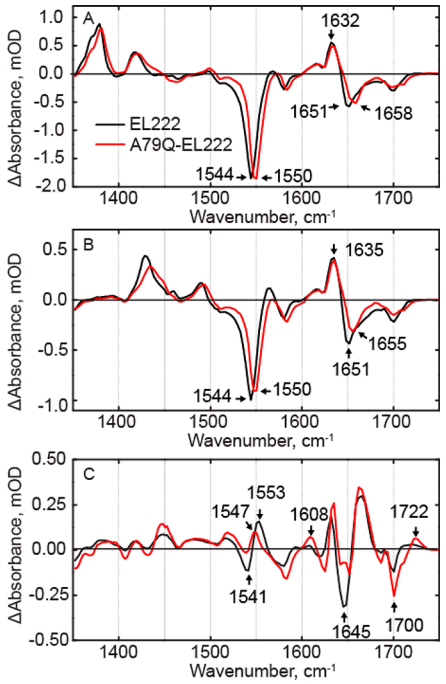

Figure 4. EAS of A79Q-EL222 from global fitting of the data showing (A) ^{1}FMN*, (B) ^{3}FMN*, and (C) A390 of EL222 and A79Q-EL222. Changes in ring modes at 1544, 1380, and 1425 cm^{-1} indicate that hydrogen bonding to FMN is restored compared to that in wild-type EL222.

(Figure 4A), the major bleach at 1544 cm^{-1} in wild-type EL222 is blue-shifted to 1550 cm^{-1}, which is closer to the frequency of this bleach in the other LOV proteins that are at 1550, 1548, and 1552 cm^{-1} in AsLOV2, YtvA, and LovK, respectively. The band at ∼1550 cm^{-1} is a delocalized ring stretching vibration, and previous ^{13}C labeling of the chromophore revealed that C2

DOI: 10.1021/acs.biochem.7b01040
Biochemistry 2018, 57, 620−630

of FMN contributes to this vibrational mode. In addition, there is a 7 cm^{-1} blue-shift from 1651 to 1658 cm^{-1} in a bleach corresponding to a protein mode. The transients at ~1635 cm^{-1} can be assigned to N117, while the lower-frequency transient is likely N107, which is hydrogen bonded to the FMN C2=O group. Similar to the other LOV proteins, the EAS for ^{3}FMN* in A79Q-EL222 is characterized by the decay of ES transients at 1381 and 1421 cm^{-1} and the rise of transients at 1433 and 1494 cm^{-1} with minimal changes in the 1600−1700 cm^{-1} region.

Interestingly, there are several differences in the A390 EAS of A79Q compared to that of the wild-type protein. There is a 6 cm^{-1} red-shift of the C4−C10a transient associated with Cys adduct formation from 1553 to 1547 cm^{-1}. This causes a decrease in the amplitude of the transient/bleach pair, while the bleach is now observed at 1541 cm^{-1} in A79Q-EL222. The transient at 1722 cm^{-1} in the mutant is assigned to FMN C4=O, which is shifted ~10 cm^{-1} from the position found in the wild-type protein and thus more similar to the position of this transient in the other LOV domain proteins, whereas in wild-type EL222, this transient is much broader. In summary, the changes in the bands assigned to the FMN ring modes between wild-type EL222 and A79Q-EL222 indicate that introduction of Q79 results in a FMN environment that more closely matches that found in the other proteins. However, protein modes in the 1600−1700 cm^{-1} region still resemble those of wild-type EL222, despite the changes in the flavin modes.

Kinetics of the LOV Photoreceptors. Kinetic parameters were determined from the same global fit of the entire data set used for EAS analysis (Table 1 and Figure 5). AsLOV2, YtvA, and LovK show the most similarity in excited singlet state decay (~2.2 ns), whereas EL222 has a slower decay of 3.3 ns. Triplet state decay rates for AsLOV2 and YtvA are nearly identical at ~10 μs, while LovK is slower at 15 μs and EL222 faster with a rate of 4.2 μs. Previous visible transient absorption studies performed on YtvA in H_2O show triplet state decay times on the order of 1−2 μs.[23,33] Because the EAS kinetics were determined in D_2O, we can conclude that the rate of triplet state decay and adduct formation occurs with a kinetic isotope effect of ~5−10 for YtvA.

Table 1. Kinetic Parameters from Global Fitting of Each Data Set

	AsLOV2	YtvA	LovK	EL222	A79Q-EL222
1FMN*	2.4 ns	2.1 ns	2.0 ns	3.3 ns	2.7 ns
3FMN*	9.5 μs	10.2 μs	15.3 μs	4.2 μs	1.9 μs
A390	long	long	long	long	long

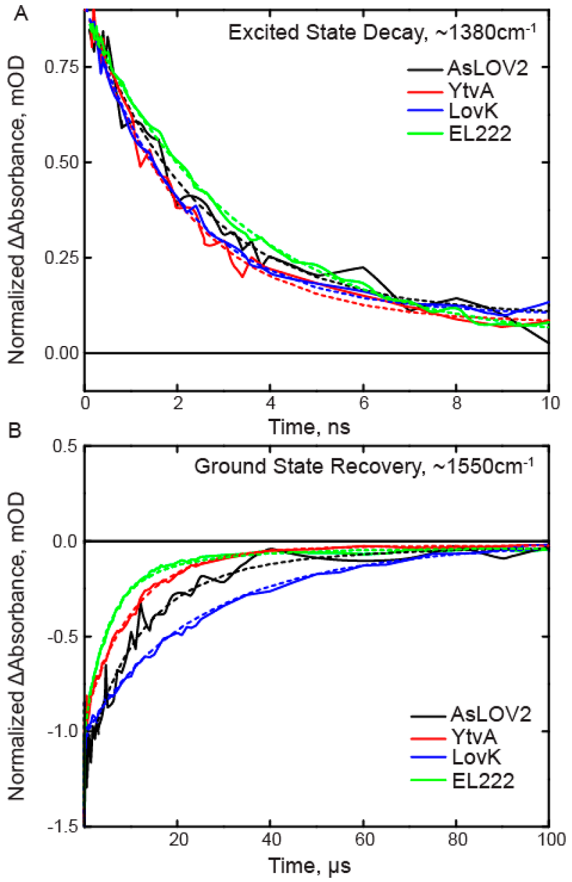

Figure 5. Excited state decay and ground state recovery kinetics of the LOV proteins fit to the sequential model. Raw data are shown as a solid line, and results of the global fit are shown as dashed lines. (A) ^{1}FMN* decay is shown on the nanosecond time scale and is extracted from the transient absorption at 1380 cm^{-1}. (B) Ground state recovery is shown on the microsecond time scale and is extracted from the main bleach at 1550 cm^{-1}. Global fits for each photoreceptor are shown as dashed lines.

Continued Structural Evolution Is Observed on the Microsecond Time Scale. Thus far, we have described the early events up to adduct formation in the LOV photocycle; however, structural evolution is also observed on a time scale of hundreds of microseconds in the TRMPS experiment, with the most dramatic changes being observed in LovK. In AsLOV2, it was shown previously that when TRMPS spectra from 100 to 400 μs are normalized to the adduct C4−C10a bleach at 1553 cm^{-1}, the magnitude of a bleach at 1625 cm^{-1} continues to increase with a submillisecond time constant, indicating a decrease in β-sheet content.[34] The transient in the ~1660 cm^{-1} region also increases on this longer time scale. A similar evolution in a bleach at 1625 cm^{-1} is observed in the YtvA TRMPS spectrum (Figure 6A), together with an increase in the magnitude of a bleach at 1642 cm^{-1} that is assigned to uncoiling of the coiled-coil helices linking the LOV domain to the STAS domain of YtvA based on studies with model coiled coils.[35] In contrast to those of AsLOV2 and YtvA, the TRMPS data for LovK (Figure 6B) and EL222 support an overall increase in β-sheet content over this longer time scale, based on an increase in transients at 1633 and 1631 cm^{-1}, respectively. The TRMPS data thus suggest significant variation in the structural dynamics of the LOV domains at longer time scales where AsLOV2 and YtvA show a loss of β-sheet content (bleach upon light state formation), whereas the β-sheet content increases in LovK and EL222 (transient).

The TRMPS spectra provide insight into the structural evolution of the photoreceptors out to ~400 μs. However, comparison of the final TRMPS spectrum with the steady state FTIR difference spectrum (Figure 7) reveals that structural

DOI: 10.1021/acs.biochem.7b01040
Biochemistry 2018, 57, 620−630

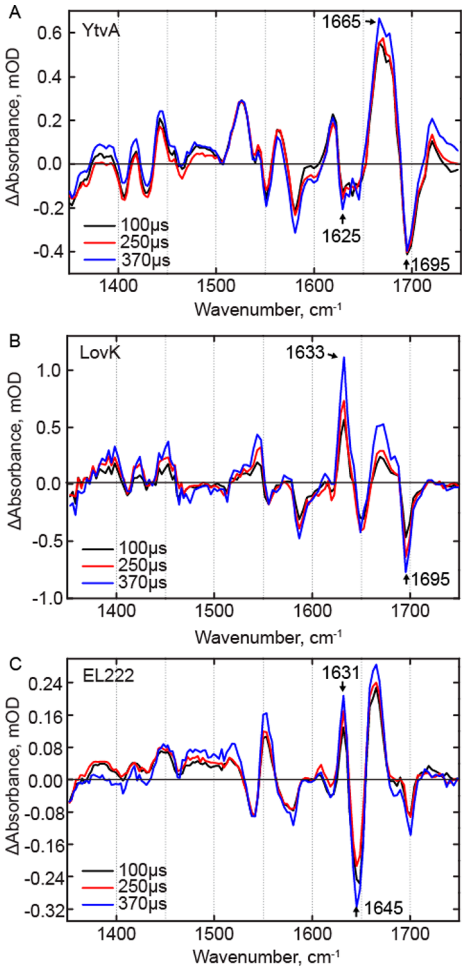

Figure 6. TRMPS spectra of the LOV photoreceptors on the microsecond time scale. Spectra after 100 μs were normalized to the adduct bleach mode at ~1550 cm^{-1} for (A) YtvA, (B) LovK, and (C) EL222.

dynamics of the proteins must occur on even longer time scales. In AsLOV2, evolution of bleaches at 1625 and 1690 cm^{-1} and a transient at 1634 cm^{-1} is observed to occur between the final TRMPS spectrum and the light minus dark (L − D) FTIR spectrum, which were previously assigned to β-sheet, Q513, and α-helix, respectively.[36,37] In the case of YtvA (Figure 7B), a bleach at 1625 cm^{-1} clearly evolves between the 370 μs TRMPS spectrum and the steady state spectrum as shown in the light−dark FTIR spectrum (Figure 7B). In EL222 (Figure 7D), the only modes that are evolving on these longer time scales are a bleach at 1683 cm^{-1} and the large transient at 1665 cm^{-1} that red-shifts to 1657 cm^{-1}.

Several differences are observed in the LovK L − D FTIR spectrum (Figure 7C) compared to the 390 μs TRMPS spectrum. Most prominent in this regard are the shoulder at 1684 cm^{-1} and the shift of the protein/flavin transient at 1663 cm^{-1}, causing the shift of the 1695 cm^{-1} bleach. In addition, both bleaches and transients in the 1400−1500 cm^{-1} region appear to blue-shift by ~10 cm^{-1} in LovK. A similar effect is observed for YtvA where a bleach at 1422 cm^{-1} is shifted to 1428 cm^{-1}. These modes are assigned to proline residues that are perturbed because of changes in the central β-sheet.[38] The L − D FTIR spectra of YtvA and LovK have been measured previously in H_2O buffer, and the data shown here agree with the previous measurements despite a few differences mainly due to experimental conditions that will be addressed in the Discussion.[26,39]

DISCUSSION

LOV activation proceeds through four major phases: a singlet excited state (i) intersystem crossing on the ~2 ns time scale to a triplet state (ii), from which a cysteine adduct is formed in ~20 μs (iii) leading to large-scale changes in protein structure on the microsecond time scale and longer. The TRMPS spectra and kinetics for each of these phases were measured and compared for four LOV photoreceptors. Further evolution beyond 400 μs is observed for each photoreceptor using FTIR difference spectroscopy. Transients at ~1380 cm^{-1} and the ground state bleaches at ~1550 cm^{-1} for all four proteins vary by no more than 10 cm^{-1} from each other, as expected for flavin modes. Each protein shares a conserved β-sheet motif, and changes in the vibrational modes assigned to the β-sheet are observed on a time scale of hundreds of microseconds. The L − D FTIR data in this work were obtained in D_2O buffer at a concentration of 1 mM. While these spectra are similar to those published previously,[26,40] there are a few differences. For example, the L − D spectrum of Bednarz et al.[26] has a well-resolved transient at ~1680 cm^{-1} that appears as a large red-shifted transient in our data. In addition, we observe a band at 1632 cm^{-1} that is not resolved in the spectrum presented by Alexandre et al.[40] These differences could be due to an H/D effect on the amide I region of the spectrum and/or the fact that the other studies were performed on dehydrated samples.

Differences between the excited state spectra are observed among the four proteins. AsLOV2, YtvA, and LovK show very similar excited state spectra and kinetics except for the protein transients in the 1600−1670 cm^{-1} region. In AsLOV2 and EL222, the transient at 1622 cm^{-1} appears as a symmetrical peak, while in YtvA and LovK, there are well-resolved shoulders on the transient. When the spectra of these three proteins are compared to that of EL222, the differences are more significant with an ~6 cm^{-1} shift in the main bleach from ~1550 to 1544 cm^{-1} that is a result of the Gln to Ala replacement in EL222, as confirmed by studies of the A79Q mutation in which the main bleach shifts from 1544 cm^{-1} in WT EL222 to 1550 cm^{-1} in A79Q-EL222. In addition, the bleach at 1652 cm^{-1} in EL222 is ~10 cm^{-1} red-shifted compared to those of the other LOV domains, which is assigned to stronger hydrogen bonding around FMN.

The singlet excited state of FMN forms within the instrument response time for each of the proteins and decays to the triplet state with a rate of ~2 ns for AsLOV2, YtvA, and LovK, while a 2-fold decrease in decay rate to 3.5 ns is observed in EL222. The reduced rate of excited state decay for EL222 has not been previously described; however, Raffelberg and co-workers reported modulation of the fluorescence quantum yield through mutation of residues interacting with the C2═O hydrogen bonding network in YtvA.[23] The triplet state decays in ~10 μs for AsLOV2 and YtvA, 15 μs for LovK, and 4.2 μs for EL222. Triplet decay rates for AsLOV2 and YtvA were previously reported to be in the range of 1−3 μs.[33,41] The latter measurements were performed in H_2O, whereas our samples were exchanged into D_2O prior to data collection. The observation of a large (5−10-fold) kinetic isotope effect for decay of the AsLOV2 and YtvA triplet states suggests that the transfer of a proton to FMN N5 occurs in the rate-limiting step leading to adduct formation, consistent with the kinetic isotope

DOI: 10.1021/acs.biochem.7b01040
Biochemistry 2018, 57, 620−630

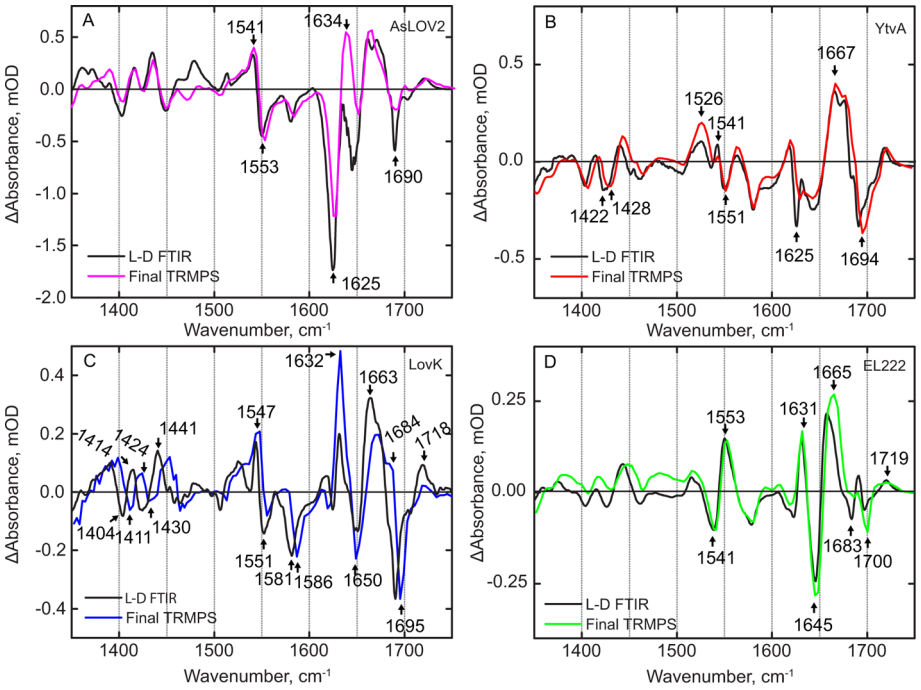

Figure 7. Comparison of latest TRMPS and steady state FTIR spectra reveal structural evolution after 400 μs. Light minus dark (L − D) FTIR difference spectra of (A) AsLOV2, (B) YtvA, (C) LovK, and (D) EL222 were measured to evaluate structural evolution on the microsecond time scale (390 μs spectrum from TRMPS) to the final steady state.

effect studies reported by Corchnoy et al.[41] In contrast, no kinetic isotope effect is observed on the decay rates for the singlet excited state, as the values obtained in our measurements are comparable to those obtained in H_2O.[11,39] Finally, the structural dynamics that occur in the microsecond to millisecond regime have not been measured in H_2O, and thus, it is not possible to assess whether these longer time-scale events are subject to a kinetic isotope effect. Using protein folding as a paradigm for the structural changes that occur between the LOV domain dark and light states, we note that while deuterium substitution has a well-accepted, albeit usually small, impact on the thermodynamics of protein folding, the effect on the rates of protein folding is complex and difficult to predict because of the multiple effects caused by the impact of deuteration on protein backbone hydrogen bonds, on protein solvent hydrogen bonds, and on the hydrophobic effect.[42−47]

The X-ray crystal structures of AsLOV2 (2V0U), YtvA (2PR5), and EL222 (3P7N) were superimposed to identify key differences in the LOV domain structure, including the orientation of the C-terminal effector domain (Figure 1). In addition, while the X-ray structure of LovK is currently unavailable, the kinetic and spectral parameters have been analyzed in the context of a sequence alignment of the four LOV domain sequences (Figure S4). The hydrogen bond network is highly conserved among the three proteins shown in Figure 1 except for EL222: while a Gln residue is hydrogen bonded to the FMN ribityl chain and the C2═O group in AsLOV2 and YtvA, in EL222 this Gln residue is replaced with an Ala residue. On the basis of sequence alignment, we propose that the homologous residue in LovK is a Gln (Figure S4). In addition to the Gln to Ala substitution in EL222, one other difference in the flavin binding pocket is the variation of Phe494, Leu106, or Val119 in AsLOV2, YtvA, or EL222, respectively. Sequence alignment (Figure S4) suggests that this residue is a Leu in LovK. F494 is notable because of its distance and conformation relative to the isoalloxazine ring, which allows for π-stacking (Figure S5).

We have rationalized some of the differences in the TRIR spectra between EL222 and the other LOV proteins by studying the A79Q mutation that slows the dark state recovery rate of EL222.[18] Despite restoring an interaction to FMN, which is evident in the shift of flavin ring C═N modes from 1544 to 1550 cm^{-1}, which is found at 1548, 1552, and 1555 cm^{-1} in AsLOV2, YtvA, and LovK, respectively, this mutant does not fully restore the LOV hydrogen bonding network. Our data suggest that Q79 does not occupy the same conformation in the flavin binding pocket and the other LOV proteins and that a hydrogen bond is disturbed rather than restored in A79Q-EL222 because of the shift in frequency from 1651 cm^{-1} in WT EL222 to 1658 cm^{-1} in A79Q-EL222, which we assign to Gln- or Asn-derived protein C═O modes that comprise the hydrogen bonding network. Another difference can be found in the kinetics of triplet decay/adduct formation in A79Q-EL222, which are faster than those of WT EL222, and it has been shown previously that mutations around the C2═O hydrogen bonding network can modulate triplet decay kinetics.[23]

The global structural changes in EL222 that lead to signaling state formation must occur faster than those that occur in YtvA and LovK, because only minor changes in IR difference spectra occur after hundreds of microseconds. Bands at 1633 cm^{-1} in LovK and 1631 cm^{-1} in EL222 assigned to the β-sheet grow in on a time scale of hundreds of microseconds, while the corresponding band in YtvA (1625 cm^{-1}) does not change on this time scale but is observed in L − D FTIR. On the microsecond to steady state time scale, the evolution of vibrational modes assigned to the β-sheet is observed. This suggests that changes due to adduct formation propagate slowly as the distance from the conserved Cys increases. The appearance of a 1625 cm^{-1} bleach in AsLOV2 and YtvA suggests a loss of β-sheet content, while the appearance of

DOI: 10.1021/acs.biochem.7b01040
Biochemistry 2018, 57, 620−630

transient bands at 1631 and 1633 cm^{-1} in EL222 and LovK, respectively, suggests an increase in β-sheet content. Significant evolution is observed in the 1400−1450 cm^{-1} region in YtvA and LovK, which we assigned on the basis of ^{15}N labeling to proline N−D modes, specifically P110 in YtvA and P118 in LovK, which are located on the β-sheet adjacent to a disordered loop (Figure S6).

On the basis of analytical ultracentrifugation and SAXS data, it was previously concluded that large-scale structural changes such as a change in oligomerization or secondary structure do not occur during activation of YtvA.[48] Our data are largely in agreement with this conclusion, where the structural changes in YtvA are likely confined to alterations in hydrogen bonding or other interactions such as salt bridges that accompany local changes in secondary structure. In addition, the microsecond to millisecond structural dynamics reported in this work agree with data from Choi et al., who reported structural changes in the Jα helices occur on the order of ∼100 μs and beyond.[28]

CONCLUSION

The LOV domain is a highly conserved flavin binding motif that couples light absorption to a variety of biological responses. In this report, we describe the structural dynamics of three full-length LOV photoreceptors, from the instantaneous formation of the excited state to the structural changes that result in the biologically relevant functional light state. Despite the high level of conservation, subtle differences are observed in excited state structure and the associated kinetics due to the specific flavin−protein interactions that are present in each photoreceptor. On the microsecond to second time scale, spectral evolution associated with large-scale structural dynamics is observed and distinct for each of the proteins measured. This work paves the way for future high-resolution spectroscopic and structural studies that aim to uncover a pathway between FMN excitation and large-scale structural changes associated with photoactivation.

ASSOCIATED CONTENT

Supporting Information

The Supporting Information is available free of charge on the ACS Publications website at DOI: 10.1021/acs.biochem.7b01040.

A table of band assignments for the four LOV photoreceptors (Table S1) and six figures, including the LOV photocycle and numbering of the isoalloxazine ring (Figure S1), kinetic traces for the excited state decay and ground state recovery together with a plot of the residuals to support the quality of data fitting (Figure S2), light minus dark FTIR spectra of unlabeled YtvA and ^{15}N-labeled YtvA (Figure S3) to support band assignments, sequence alignment of the LOV domains to show sequence conservation between LovK, for which no X-ray structure is available, and the three other photoreceptors (Figure S4), and overlays of the AsLOV2, YtvA, and EL222 structures showing the position of F494 in AsLOV2 (Figure S5) and a proline residue on the LOV β-sheet (P110 in YtvA) (Figure S6) (PDF)

AUTHOR INFORMATION

Corresponding Authors

*E-mail: s.meech@uea.ac.uk.

*E-mail: peter.tonge@stonybrook.edu.

ORCID

James N. Iuliano: 0000-0003-1213-3292
Agnieszka A. Gil: 0000-0001-7583-3080
Sergey P. Laptenok: 0000-0002-6468-3010
Andras Lukacs: 0000-0001-8841-9823
Markus Fischer: 0000-0001-7243-4199
Jarrod B. French: 0000-0002-6762-1309
Stephen R. Meech: 0000-0001-5561-2782
Peter J. Tonge: 0000-0003-1606-3471

Present Address

@S.P.L.: Biological and Environmental Science and Engineering Division, King Abdullah University of Science and Technology, P.O. Box 4700, Thuwal 23955-6900, Kingdom of Saudi Arabia.

Funding

This study was supported by the EPSRC (EP/G002916 to S.R.M.) and the National Science Foundation (NSF) (CHE-1223819 to P.J.T.). J.N.I. was supported by a National Institutes of Health Chemistry-Biology Interface training grant (T32GM092714). A.L. is a Bolyai János Research Fellow and was supported by OTKA NN113090. J.A. was supported by the NSF REU program at Stony Brook University (NSF-CHE-1358959). S.A.H.A. was a Fulbright Scholar and gratefully acknowledges support from the Fulbright Program. J.T.C. was supported by the IMSD-MERGE Program at Stony Brook University (5R25GM103962-04).

Notes

The authors declare no competing financial interest.

ACKNOWLEDGMENTS

The authors are grateful to STFC for access to the ULTRA laser facility. The authors also are grateful to Professor Ray Owens and Anil Verma for assistance in protein preparation and access to the Oxford Protein Production Facility.

REFERENCES

(1) Herrou, J., and Crosson, S. (2011) Function, structure and mechanism of bacterial photosensory LOV proteins. *Nat. Rev. Microbiol. 9*, 713−723.

(2) Crosson, S., and Moffat, K. (2002) Photoexcited Structure of a Plant Photoreceptor Domain Reveals a Light-Driven Molecular Switch. *Plant Cell 14*, 1067−1075.

(3) Nozaki, D., Iwata, T., Ishikawa, T., Todo, T., Tokutomi, S., and Kandori, H. (2004) Role of Gln1029 in the photoactivation processes of the LOV2 domain in Adiantum phytochrome3. *Biochemistry 43*, 8373−8379.

(4) Harper, S. M. (2003) Structural Basis of a Phototropin Light Switch. *Science (Washington, DC, U. S.) 301*, 1541−1544.

(5) Herrou, J., and Crosson, S. (2011) Function, structure and mechanism of bacterial photosensory LOV proteins. *Nat. Rev. Microbiol. 9*, 713−723.

(6) Christie, J. M., Gawthorne, J., Young, G., Fraser, N. J., and Roe, A. J. (2012) LOV to BLUF: Flavoprotein contributions to the optogenetic toolkit. *Mol. Plant 5*, 533−544.

(7) *The PyMOL Molecular Graphics System*, version 1.8, Schrodinger, LLC, Portland, OR.

(8) Swartz, T. E., Corchnoy, S. B., Christie, J. M., Lewis, J. W., Szundi, I., Briggs, W. R., and Bogomolni, R. A. (2001) The Photocycle of a Flavin-binding Domain of the Blue Light Photoreceptor Phototropin. *J. Biol. Chem. 276*, 36493−36500.

(9) Winkler, A., Barends, T. R. M., Udvarhelyi, A., Lenherr-Frey, D., Lomb, L., Menzel, A., and Schlichting, I. (2015) Structural details of light activation of the LOV2-based photoswitch PA-Rac1. *ACS Chem. Biol. 10*, 502−509.

DOI: 10.1021/acs.biochem.7b01040
Biochemistry 2018, 57, 620−630

(10) Guntas, G., Hallett, R. a., Zimmerman, S. P., Williams, T., Yumerefendi, H., Bear, J. E., and Kuhlman, B. (2015) Engineering an improved light-induced dimer (iLID) for controlling the localization and activity of signaling proteins. *Proc. Natl. Acad. Sci. U. S. A. 112*, 112−117.
(11) Alexandre, M. T. A., Domratcheva, T., Bonetti, C., van Wilderen, L. J. G. W., van Grondelle, R., Groot, M.-L., Hellingwerf, K. J., and Kennis, J. T. M. (2009) Primary reactions of the LOV2 domain of phototropin studied with ultrafast mid-infrared spectroscopy and quantum chemistry. *Biophys. J. 97*, 227−237.
(12) Pfeifer, A., Majerus, T., Zikihara, K., Matsuoka, D., Tokutomi, S., Heberle, J., and Kottke, T. (2009) Time-Resolved Fourier Transform Infrared Study on Photoadduct Formation and Secondary Structural Changes within the Phototropin LOV Domain. *Biophys. J. 96*, 1462−1470.
(13) Gil, A. A., Laptenok, S. P., French, J. B., Iuliano, J. N., Lukacs, A., Hall, C. R., Sazanovich, I. V., Greetham, G. M., Bacher, A., Illarionov, B., Fischer, M., Tonge, P. J., and Meech, S. R. (2017) Femtosecond To Millisecond Dynamics Of Light Induced Allostery In The Avena Sativa Lov Domain. *J. Phys. Chem. B 121*, 1010−1019.
(14) Konold, P. E., Mathes, T., Weiβenborn, J., Groot, M. L., Hegemann, P., and Kennis, J. T. M. (2016) Unfolding of the C-Terminal Jα Helix in the LOV2 Photoreceptor Domain Observed by Time-Resolved Vibrational Spectroscopy. *J. Phys. Chem. Lett. 7*, 3472−3476.
(15) Möglich, A., and Moffat, K. (2007) Structural Basis for Light-dependent Signaling in the Dimeric LOV Domain of the Photosensor YtvA. *J. Mol. Biol. 373*, 112−126.
(16) Purcell, E. B., McDonald, C. A., Palfey, B. A., and Crosson, S. (2010) An analysis of the solution structure and signaling mechanism of LovK, a sensor histidine kinase integrating light and redox signals. *Biochemistry 49*, 6761−6770.
(17) Nash, A. I., McNulty, R., Shillito, M. E., Swartz, T. E., Bogomolni, R. a, Luecke, H., and Gardner, K. H. (2011) Structural basis of photosensitivity in a bacterial light-oxygen-voltage/helix-turn-helix (LOV-HTH) DNA-binding protein. *Proc. Natl. Acad. Sci. U. S. A. 108*, 9449−54.
(18) Zoltowski, B. D., Motta-mena, L. B., and Gardner, K. H. (2013) Blue Light-Induced Dimerization of a Bacterial LOV − HTH DNA-Binding Protein. *Biochemistry 52*, 6653−6661.
(19) Salomon, M., Christie, J. M., Knieb, E., Lempert, U., and Briggs, W. R. (2000) Photochemical and mutational analysis of the FMN-binding domains of the plant blue light receptor, phototropin. *Biochemistry 39*, 9401−9410.
(20) Losi, A., Polverini, E., Quest, B., and Gärtner, W. (2002) First evidence for phototropin-related blue-light receptors in prokaryotes. *Biophys. J. 82*, 2627−2634.
(21) Nash, A. I., McNulty, R., Shillito, M. E., Swartz, T. E., Bogomolni, R. a, Luecke, H., and Gardner, K. H. (2011) Structural basis of photosensitivity in a bacterial light-oxygen-voltage/helix-turn-helix (LOV-HTH) DNA-binding protein. *Proc. Natl. Acad. Sci. U. S. A. 108*, 9449−54.
(22) Zayner, J. P., and Sosnick, T. R. (2014) Factors that control the chemistry of the LOV domain photocycle. *PLoS One 9*, e87074.
(23) Raffelberg, S., Mansurova, M., Gärtner, W., and Losi, A. (2011) Modulation of the photocycle of a LOV domain photoreceptor by the hydrogen-bonding network. *J. Am. Chem. Soc. 133*, 5346−5356.
(24) Eitoku, T., Nakasone, Y., Matsuoka, D., Tokutomi, S., and Terazima, M. (2005) Conformational dynamics of phototropin 2 LOV2 domain with the linker upon photoexcitation. *J. Am. Chem. Soc. 127*, 13238−13244.
(25) Nakasone, Y., Eitoku, T., Matsuoka, D., Tokutomi, S., and Terazima, M. (2007) Dynamics of Conformational Changes of Arabidopsis Phototropin 1 LOV2 with the Linker Domain. *J. Mol. Biol. 367*, 432−442.
(26) Bednarz, T., Losi, A., Gärtner, W., Hegemann, P., and Heberle, J. (2004) Functional variations among LOV domains as revealed by FT-IR difference spectroscopy. *Photochem. Photobiol. Sci. 3*, 575−579.
(27) Losi, A., Ghiraldelli, E., Jansen, S., and Gärtner, W. (2005) Mutational effects on protein structural changes and interdomain interactions in the blue-light sensing LOV protein YtvA. *Photochem. Photobiol. 81*, 1145−1152.
(28) Choi, S., Nakasone, Y., Hellingwerf, K. J., and Terazima, M. (2016) Photochemical Reactions of the LOV and LOV-Linker Domains of the Blue Light Sensor Protein YtvA. *Biochemistry 55*, 3107−3115.
(29) Greetham, G. M., Sole, D., Clark, I. P., Parker, A. W., Pollard, M. R., and Towrie, M. (2012) Time-resolved multiple probe spectroscopy. *Rev. Sci. Instrum. 83*, 103107.
(30) Snellenburg, J. J., Laptenok, S. P., Seger, R., Mullen, K. M., and van Stokkum, I. H. M. (2012) Glotaran: A *Java*-Based Graphical User Interface for the *R* Package TIMP. *Journal of Statistical Software 49*, n/a DOI: 10.18637/jss.v049.i03.
(31) Kondo, M., Nappa, J., Ronayne, K. L., Stelling, A. L., Tonge, P. J., and Meech, S. R. (2006) Ultrafast vibrational spectroscopy of the flavin chromophore. *J. Phys. Chem. B 110*, 20107−20110.
(32) Haigney, A., Lukacs, A., Zhao, R. K., Stelling, A. L., Brust, R., Kim, R. R., Kondo, M., Clark, I., Towrie, M., Greetham, G. M., Illarionov, B., Bacher, A., Römisch-Margl, W., Fischer, M., Meech, S. R., and Tonge, P. J. (2011) Ultrafast infrared spectroscopy of an isotope-labeled photoactivatable flavoprotein. *Biochemistry 50*, 1321−1328.
(33) Song, S. H., Madsen, D., Van Der Steen, J. B., Pullman, R., Freer, L. H., Hellingwerf, K. J., and Larsen, D. S. (2013) Primary photochemistry of the dark- and light-adapted states of the YtvA protein from bacillus subtilis. *Biochemistry 52*, 7951−7963.
(34) Buttani, V., Losi, A., Polverini, E., and Gärtner, W. (2006) Blue news: NTP binding properties of the blue-light sensitive YtvA protein from Bacillus subtilis. *FEBS Lett. 580*, 3818−3822.
(35) Reisdorf, W. C., and Krimm, S. (1996) Infrared amide I′ band of the coiled coil. *Biochemistry 35*, 1383−1386.
(36) Herman, E., Sachse, M., Kroth, P. G., and Kottke, T. (2013) Blue-light-induced unfolding of the Jα helix allows for the dimerization of aureochrome-LOV from the diatom Phaeodactylum tricornutum. *Biochemistry 52*, 3094−3101.
(37) Banerjee, A., Herman, E., Serif, M., Maestre-Reyna, M., Hepp, S., Pokorny, R., Kroth, P. G., Essen, L.-O., and Kottke, T. (2016) Allosteric communication between DNA-binding and light-responsive domains of diatom class I aureochromes. *Nucleic Acids Res. 44*, 5957.
(38) Barth, a. (2000) The infrared absorption of amino acid side chains. *Prog. Biophys. Mol. Biol. 74*, 141−173.
(39) Alexandre, M. T. A., Purcell, E. B., Van Grondelle, R., Robert, B., Kennis, J. T. M., and Crosson, S. (2010) Electronic and protein structural dynamics of a photosensory histidine kinase. *Biochemistry 49*, 4752−4759.
(40) Alexandre, M. T. A., Van Grondelle, R., Hellingwerf, K. J., and Kennis, J. T. M. (2009) Conformational heterogeneity and propagation of structural changes in the LOV2/Jα domain from Avena sativa phototropin 1 as recorded by temperature-dependent FTIR spectroscopy. *Biophys. J. 97*, 238−247.
(41) Corchnoy, S. B., Swartz, T. E., Lewis, J. W., Szundi, I., Briggs, W. R., and Bogomolni, R. A. (2003) Intramolecular proton transfers and structural changes during the photocycle of the LOV2 domain of phototropin 1. *J. Biol. Chem. 278*, 724−731.
(42) Kuhlman, B., and Raleigh, D. P. (1998) Global analysis of the thermal and chemical denaturation of the N-terminal domain of the ribosomal protein L9 in H_2O and D_2O. Determination of the thermodynamic parameters, ΔH°, ΔS°, and ΔC°_p. *Protein Sci. 7*, 2405−2412.
(43) Krantz, B. A., Moran, L. B., Kentsis, A., and Sosnick, T. R. (2000) D/H amide kinetic isotope effects reveal when hydrogen bonds form during protein folding. *Nat. Struct. Biol. 7*, 62−71.
(44) Creswell, C. J., and Allred, A. L. (1962) The Strengths Of Hydrogen Bonds Formed By Protium and Deuterium. *J. Am. Chem. Soc. 84*, 3966−3967.

DOI: 10.1021/acs.biochem.7b01040
Biochemistry 2018, 57, 620−630

(45) Makhatadze, G. I., Clore, G. M., and Gronenborn, A. M. (1995) Solvent isotope effect and protein stability. *Nat. Struct. Biol. 2*, 852−855.
(46) Itzhaki, L. S., and Evans, P. A. (1996) Solvent isotope effects on the refolding kinetics of hen egg-white lysozyme. *Protein Sci. 5*, 140−146.
(47) Kresheck, G. C., Schneider, H., and Scheraga, H. a. (1965) The effect of D2O on the thermal stability of proteins. Thermodynamic parameters for the transfer of model compounds from H2O to D2O. *J. Phys. Chem. 69*, 3132−3144.
(48) Jurk, M., Dorn, M., Kikhney, A., Svergun, D., Gartner, W., and Schmieder, P. (2010) The Switch that Does Not Flip: The Blue-Light Receptor YtvA from Bacillus subtilis Adopts an Elongated Dimer Conformation Independent of the Activation State as Revealed by a Combined AUC and SAXS Study. *J. Mol. Biol. 403*, 78−87.

DOI: 10.1021/acs.biochem.7b01040
Biochemistry 2018, 57, 620−630